Surface & Coatings Technology 206 (2012) 4249–4255

Contents lists available at SciVerse ScienceDirect

Surface & Coatings Technology

journal homepage: www.elsevier.com/locate/surfcoat

Residual stresses in cold spray Al coatings: The effect of alloying and of process parameters

K. Spencer [a,1], V. Luzin [b], N. Matthews [c], M.-X. Zhang [a,1,*]

[a] Division of Materials, School of Mechanical and Mining Engineering, The University of Queensland, QLD 4072, Australia
[b] The Bragg Institute, Australian Nuclear Science and Technology Organisation Locked Bag 2001 Kirrawee DC NSW 2232, Australia
[c] Rosebank Engineering Pty Ltd, 836 Mountain Highway, Bayswater, VIC 3153, Australia

ARTICLE INFO

Article history:
Received 2 January 2012
Accepted in revised form 13 April 2012
Available online 24 April 2012

Keywords:
Cold spray
Kinetic metallization
Residual stress
Internal stress
Neutron diffraction

ABSTRACT

Al and Al alloy cold spray coatings were deposited on Mg substrates using two different cold spray systems – a Kinetic Metallization system (convergent barrel, sonic nozzle) and a CGT system (convergent-divergent barrel, supersonic nozzle). The residual stress profiles in the coatings were measured using neutron diffraction with high spatial resolution. In the first part of the study, the residual stress profile in pure Al coatings was compared when sprayed using the Kinetic Metallization system (using both helium and nitrogen as the driving gas), and with the CGT system using nitrogen gas. In this way the effect of impact velocity and process temperature was studied. In the second part of the study, the residual stress profile was compared in coatings of pure Al, 7075 Al and 6061 Al sprayed using the same process conditions in the CGT system. The residual stress profiles depend more on the alloy content, *i.e.* intrinsic resistance to plastic deformation, than on the processing conditions, and this is interpreted using a simple model that incorporates the effect of peening stresses in the cold spray process.

1. Introduction

The cold spray coating process is an emerging technique for depositing coatings in the solid state. In this process the feedstock powder, which usually comprises a metal powder as its main component, is injected into a gas stream and accelerated to a speed of ~500-1000 m/s, and is impacted onto a metallic substrate. Extensive plastic deformation of the particles under pressure generates new interfaces with conformal contact, enabling metallic bonding and the build-up of a coating. The bond strength and durability of the coating are determined in part by the residual stresses arising from the peening process [1–3], when the metal particles deform on impact. The residual stress accumulation during this process is not easily predicted with a high degree of accuracy, though at the surface the residual stress is usually compressive due to the peening process [4].

Previous work comparing the measured residual stresses in Cu and Al coatings showed that the magnitude of the residual stress depends on the degree of plastic deformation, in addition to the strength level and elastic modulus of the coating and substrate materials [5]. The results were rationalised using a simple model based on the accumulation of residual stress in the shot peening process [6–8]. This raised questions about the relative importance of material properties *vs.* process parameters such as impact temperature and pressure, in the accumulation of residual stress.

The present work addresses these questions as follows. The residual stress profiles were measured in a variety of Al and Al alloy coatings sprayed on an Mg substrate, using two different cold spray processes: sonic and supersonic cold spray. This enabled the same material to be sprayed with significantly different process conditions. In addition, different alloys were sprayed using the same process conditions using supersonic cold spray. The residual stress profiles in each case were measured using high-resolution neutron diffraction. Other properties such as the density and elastic modulus of the deposited coatings were measured, to further understand the deformation process that leads to coating build-up.

The residual stress accumulation in Al cold spray coatings is of interest since it can be difficult to form dense Al coatings, due to the low density of Al and the resultant low impact pressure. The case of Al coatings on an Mg substrate is studied since this a system considered for commercial application of cold spray, both for coatings and for repair [9,10]. Studying only Al alloys with a similar Young's modulus enables discussion of the stress profiles independent of this parameter.

2. Experimental procedure

2.1. Cold spray

The first cold spray process used was a Kinetic Metallization (KM) system, a commercial cold spray variant that uses a convergent barrel nozzle, manufactured by Inovati in the USA. Operated under choked

* Corresponding author. Tel.: +61 7 3346 8709; fax: +61 3365 3888.
E-mail address: mingxing.zhang@uq.edu.au (M.-X. Zhang).
[1] ARC Centre of Excellence for Design in Light Metals.

0257-8972/$ – see front matter © 2012 Elsevier B.V. All rights reserved.
doi:10.1016/j.surfcoat.2012.04.034

flow conditions, the gas speed through the nozzle barrel is ~Mach 1. The resultant nozzle gas speed will depend on the gas used (helium or nitrogen), and on the process conditions as given in Table 1. The nozzle gas speeds are calculated using isentropic ideal gas relations at Mach 1 [11], and were verified based on measured gas flow rates. Using helium gas results in a much higher sonic velocity than nitrogen, since helium gas has a lower molecular weight and higher specific heat ratio than nitrogen.

The second cold spray system used was a CGT Kinetiks 4000, another commercially-available cold spray variant manufactured by Cold Gas Technologies in Germany. This system uses a convergent-divergent nozzle to produce supersonic conditions beyond the nozzle throat. Only nitrogen gas was used with this system, though the high gas driving pressure and Mach number of ~2–2.5 generally results in higher particle exit velocities than the KM system operating with helium, for a given particle size. The two cold spray systems will be referred to as KM and CGT respectively.

The substrate used was a ZE41A Mg alloy, with a grain size close to 30 μm. The substrate samples were cut into 3 mm thick square coupons, 30 mm x 30 mm, to produce a state of balanced biaxial plane stress at the centre of the sample, where the stress measurements were made. They were cleaned with 1200 grit SiC paper and rinsed with ethanol immediately before spraying. The commercial-purity Al and Al alloys powders were spherical and produced by gas atomisation. For the Al alloys larger particle size powders were used, as it was not possible to obtain finer particle sizes.

The temperature given in Table 1 was measured immediately upstream of the nozzle throat, and is taken as the gas stagnation temperature for both helium (He) and nitrogen (N_2). This temperature, the gas stagnation pressure, and the gas properties were used to estimate the exit velocity of the particles from the nozzle, using a 1-dimensional isentropic model based on that of Dykhuizen and Smith [11]. The velocity was integrated along the nozzle barrel, and the particle drag coefficient was calculated according to the local Reynolds number, using Henderson's correlation [12]. In the case of the samples sprayed using the supersonic CGT system, the particle exit velocities were calculated using the commercially-available computational fluid dynamic code FLUENT 3D. Only the particle exit velocities will be given.

2.2. Measurement of coating properties

Specimens were cut from the coatings in the shape of a parallelepiped with flat and parallel sides, using spark cutting. These were used to measure density with an Archimedes balance, and to measure the Young's modulus of the coatings using both the impulse excitation technique [13] and the four point bending technique [14], which were in good agreement. The Young's modulus values obtained using the two different techniques varied by no more than ± 1 GPa, which provided some confidence in the accuracy of the results. Only the values obtained using impulse excitation are reported here.

The average plastic strain of the particles in the coating was estimated by examining metallographic sections parallel and transverse to the spray traverse direction, chemically etched to reveal the particle boundaries; the impact direction is vertical in all sections. The spherical particles were assumed to deform into an oblate spheroid on impact, *i.e.* uniaxial compression. The deformed particles appear as an ellipse when sectioned in the metallographic plane, with the minor axis parallel to the impact direction. These elliptical sections will have the same aspect ratio as the particle, regardless of where the plane cuts the particle [15]. The particle aspect ratio was then used to calculate the average plastic strain. At least 50 measurements were made for each direction, for each condition. This technique is considered a rough estimate at best, in the absence of any better measure of particle deformation.

Table 1
Materials and process parameters used for cold spray.

	Powder Material	Cold Spray Process	Average Particle Size (μm)	Driving Gas	Driving Pressure (kPa)	Nozzle Temperature (°C)	Nozzle Gas Speed (m/s)
1	Pure Al	KM	15	He	620	132	1025
2	Pure Al	KM	15	He	620	77	950
3	Pure Al	KM	15	N_2	758	217	412
4	Pure Al	CGT	15	N_2	3850	550	–
5	6061 Al	CGT	45	N_2	3850	400	–
6	7075 Al	CGT	45	N_2	3850	400	–

2.3. Neutron diffraction stress measurements

The neutron diffraction residual stresses measurements were performed on the KOWARI strain scanner at the ANSTO OPAL research reactor.[2] In this work a gauge volume with fine spatial resolution was used, with dimensions of ~0.5x0.5x18 mm. This volume was chosen to balance two competing factors: it should be small enough to provide the necessary through-thickness resolution and avoid edge effects, but it must be large enough to produce a count rate sufficiently high such that strains can be measured with a statistical uncertainty better than $5x10^{-5}$, within a practical measurement time.

In order to optimise localisation of the gauge volume, a 90° geometry ($2\theta_B \sim 90°$) was chosen and to maintain it, both the take-off angle $2\theta_M$ of the Si (400) monochromator and the wavelength were varied according to the material, as summarised in Table 2.

The measurements were done in several different through-thickness locations to cover the entire sample thickness, forming a line profile with 0.3 mm spacing between points. For each measurement point, d-spacings (diffraction peak positions) were measured in the two principle directions, normal to the surface and in-plane. From the measured d-spacings, in-plane stresses were calculated using the assumption of a balanced biaxial plane stress state, following the procedure described in [16]. The diffraction elastic constants used for stress calculation were computed using the self-consistent method of Kröner [17], and are reported in Table 2.

To separate stresses originating from the cold spray process from pre-existing stresses (*e.g.* residual stress from cold rolling of the substrate), neutron stress measurements were done on the uncoated substrate. They were treated as separate samples and measured using the same procedure. In subsequent data analysis, the stress profiles measured in uncoated substrates were subtracted from the stress profiles of the coated samples, as illustrated in Fig. 1. The idea was to obtain the residual stress profile due solely to the cold spray process. The residual stress in the uncoated substrate is likely due to the casting process, and as such, is not of interest in the present context.

2.4. Fitting of residual stress profiles

The residual stress profiles were interpreted by fitting them using Tsui and Clyne's progressive coating deposition model [18]. Although originally developed to model the residual stress accumulation in thermal spray coatings, this model has been found to work equally well for cold spray coatings [5]. Two components of the spray process are accounted for separately using two different fitting parameters:

1. The first fitting parameter arises from the coating deposition process being considered as the formation of a new layer on the top of the system comprising all of the previously sprayed layers, plus the substrate. This new layer is formed with a characteristic deposition stress σ_d. For cold spray coatings this stress is compressive, characteristic of a peening process.

[2] Australian Nuclear Science and Technology Organisation (ANSTO), Lucas Heights, New South Wales, 2234, Australia.

Table 2
Instrument settings and material constants for the measured reflections.

Reflection	d, Å	$2\theta_M$	λ, Å	$2\theta_B$	S_1, TPa^{-1}	½ S_2, TPa^{-1}
Mg (211)	1.03	65.0°	1.36	90.1°	−6.55	28.94
Al (311)	1.22	79.8°	1.72	89.5°	−5.16	19.57

2. In most cases the spray is performed above room temperature. After coating deposition the coating and substrate will cool to room temperature, and a thermal misfit term $\Delta\varepsilon_{th}$ is needed to account for any thermal expansion coefficient mismatch between the substrate and coating materials, where $\Delta\varepsilon_{th} = \Delta\alpha\Delta T$. The significance of this term depends on the cooling range and difference in thermal expansion coefficients between the coating and substrate materials.

Analysis of the experimentally measured stress profiles in terms of the model allows separation of σ_d and $\Delta\varepsilon_{th}$, and their relative significance can be determined for a given coating-substrate system quantitatively. This separation can be used to assess the importance of the thermal *vs.* kinetic (peening) components of the coating process, and the sensitivity of a given system to the accumulation of residual stress. Also, when a particular spraying process is characterized by σ_d and $\Delta\varepsilon_{th}$ parameters, this can be used for prediction of stresses in other systems, *e.g.* with different thickness or different materials.

3. Results

The microstructure of the different pure Al coatings is shown in Fig. 2 (A-D). The etchant attacks mainly the particle boundaries in these coatings, but there is some minor pitting of the grain boundaries within the particles. The overall appearance of the deformed structure is similar for the four different spray conditions. The pure Al coating sprayed using the CGT process (D) appears to have less porosity, though drawing conclusions from metallographic sections is difficult as porosity varies spatially throughout the coating.

The two alloy coatings sprayed using the CGT process are shown in Fig. 2 E and F. In the alloy coatings, the chemical etchant reveals both the particle boundaries and the grain boundaries contained therein. Having the deformed grain boundaries revealed makes it easier to visualise the deformation of the particle. Macroscopically, the deformation appears uniform within the particles.

A better measure of the coating compaction is the density and Young's modulus of the coatings reported as a percentage of their equivalent bulk values, as given in Table 3. Defects present in the coatings such as pores and cracks have a different effect on density and Young's modulus: while density is a measure of the volume fraction of the porosity, the Young's modulus is not only sensitive to the porosity, but also to the quality of the particle-to-particle contact. There are a few key points:

1. The KM coatings sprayed using He at the two different temperatures have the same porosity and Young's modulus.
2. The KM coating sprayed using N_2 has the same density as those sprayed using He, but a lower Young's modulus
3. All of the CGT coatings have a higher density and Young's modulus than the KM coatings

The through-thickness residual stress profiles for the coatings and Mg substrates are shown in Fig. 3. The three pure Al KM coatings (A-C) have similar stress profiles, with a small residual compressive stress at the coating surface. The pure Al CGT coating has a very different profile: there is a small residual tensile stress at the coating surface, which is an indication that thermal mismatch has a significant effect on the residual stress profile in this coating.

The Al alloy coatings sprayed using the CGT system have similar residual stress profiles, as shown Fig. 3 (D-F), to the pure Al KM coatings, but the magnitude of the residual stress is higher.

4. Discussion

The absolute values of residual shown in Fig. 3 do not appear very high. However, the significance of residual stress on coating delamination depends on the interfacial bond strength. Furthermore, the sign of the stress gradient in the coating and substrate are important. When they are opposite (as they are in all of the samples with the exception of the pure Al CGT sample), the residual stress generates a pure Mode I crack opening at the interface on debonding [19]. Interfacial shear bond strengths of pure Al coatings deposited on Mg and Al substrates have been measured to be ~30 MPa, and about 40 MPa for Al alloy coatings [20–22]. As a result, in the case of thick coatings like those in the present work, the residual stress can easily approach that needed to debond the coating. To overcome the dependence of residual stress on coating (and substrate) thickness, we employ the progressive deposition model discussed below. This enables a discussion of the residual stress state in terms of two parameters that are independent of sample geometry.

The fitting results of Tsui and Clyne's progressive deposition model [18] given in Table 4 provide a means to quantitatively interpret the residual stress profiles, by separating the two sources of the residual stress — deposition stress and thermal mismatch. It is more convenient to interpret thermal mismatch in terms of strain, so the deposition stress is expressed in terms of strain as $\Delta\varepsilon_d = 2\sigma_d/E_d$, where E_d is the coating Young's modulus. Although equal $\Delta\varepsilon_d$ and $\Delta\varepsilon_{th}$ numbers don't determine the shape of the stress profiles to the same extent, the ratio between the two indicates which process is dominant. For all samples except the CGT pure Al, the stress profiles were fit almost entirely by varying σ_d, with only a minor contribution

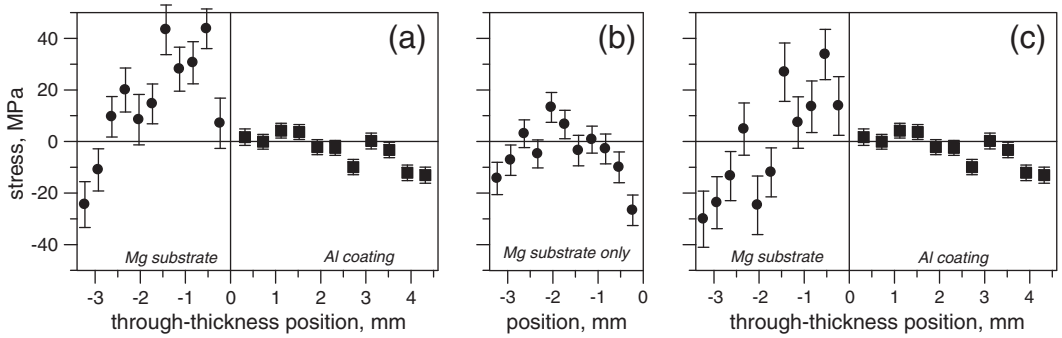

Fig. 1. Example of data treatment on the sample with a pure Al coating, sprayed using the KM system using He at 132 °C: (A) as-measured stress profile in the coated sample, (B) stress profile in the uncoated substrate, and (C) residual stress profile, due only to the cold spray process.

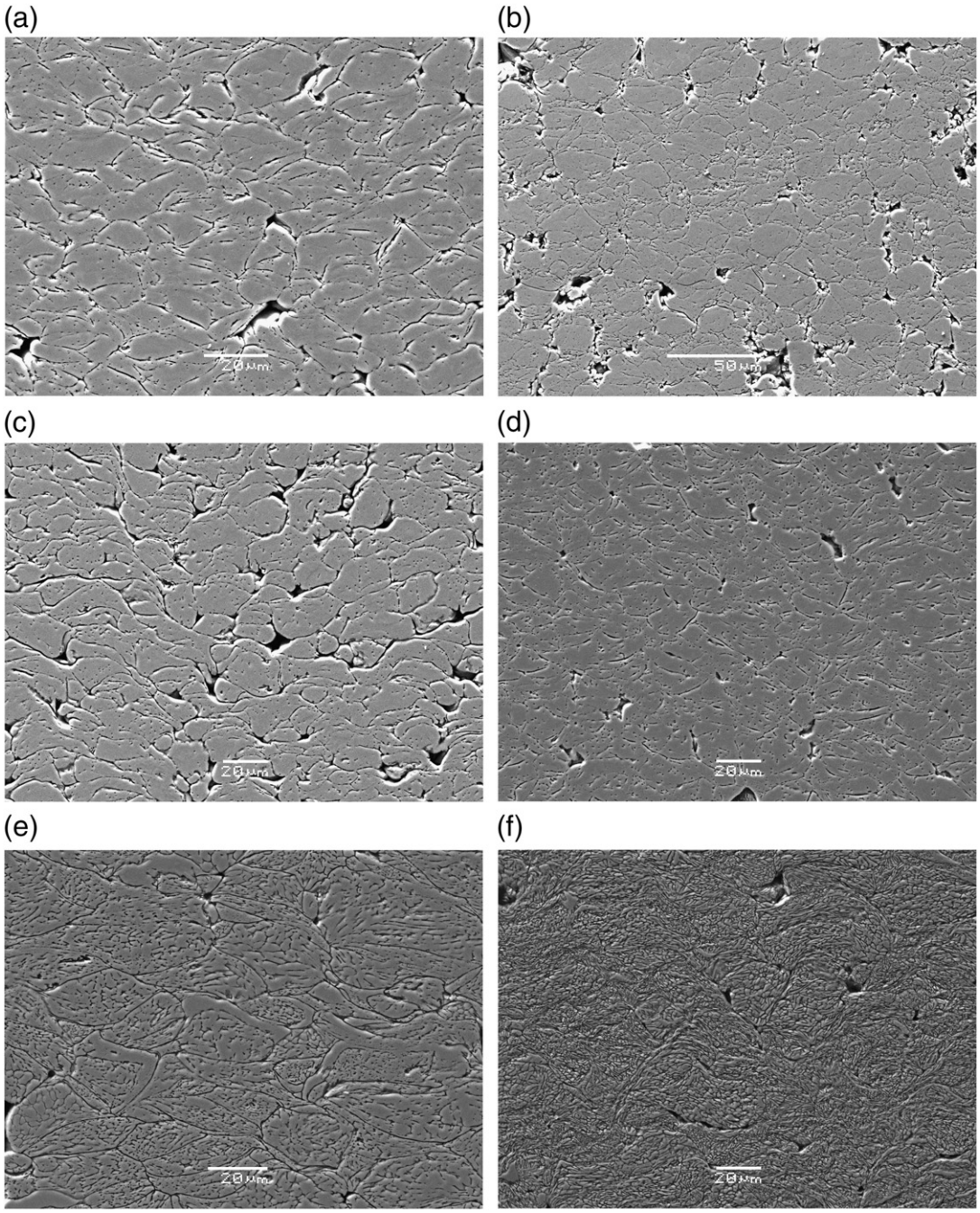

Fig. 2. Etched metallographic sections of the Al coatings. Direction of the spray nozzle travel is normal to the page. (A) KM Pure Al, He 132°C (B) KM Pure Al, He, 77°C (C) KM Pure Al, N_2 217°C (D) CGT Pure Al (E) CGT 6061Al (F) CGT 7075Al.

made by $\Delta\varepsilon_{th}$. This confirms that the stress distributions in Fig. 3 are governed mainly by the peening process, with the thermal expansion mismatch having a secondary contribution. For the CGT alloy coatings the peening stress is greatly dominant, while in the case of the CGT pure Al sample, thermal stress is overriding the peening process.

Table 3
Coating density and Young's modulus as a percentage of their equivalent bulk values.

	Coating	Impact Strain	% Bulk Density	% Bulk Young's Modulus
1	KM Al (He; 132 °C)	0.47 ± 0.16	94. 6 ± 0.4	80.9 ± 0.7
2	KM Al (He; 77 °C)	0.43 ± 0.17	95.1 ± 0.4	81.4 ± 0.7
3	KM Al (N_2; 217 °C)	0.47 ± 0.17	94.1 ± 2.0	66.6 ± 1.3
4	CGT Al	0.47 ± 0.16	98.0 ± 0.6	92.6 ± 1.7
5	CGT 6061Al	0.53 ± 0.23	96.6 ± 0.6	92.2 ± 1.7
6	CGT 7075Al	0.49 ± 0.22	98.5 ± 1.1	95.1 ± 1.4

The thermal mismatch stress depends on the choice of substrate material and sample thickness, and could be eliminated experimentally by using an Al substrate. Furthermore, although the effect of the thermal expansion coefficient (CTE) on residual stress state is straightforward, when thermal mismatch $\Delta\varepsilon_{th} = \Delta\alpha\Delta T$ is given and the thicknesses of the substrate and the coating are known, then the contribution to the stress profile can be calculated using linear elasticity theory. In the present study the thermal mismatch term is not discussed in the data analysis because it does not reveal any new information, other than the difference in CTE of the substrate and the coating (which is known anyway) and an integral drop in temperature. Instead, the deposition stress is focused and emphasised, which is the characteristics of the cold spray process and contains unique information and new scientific knowledge. We stress again that the absolute value of the residual stresses measured will depend

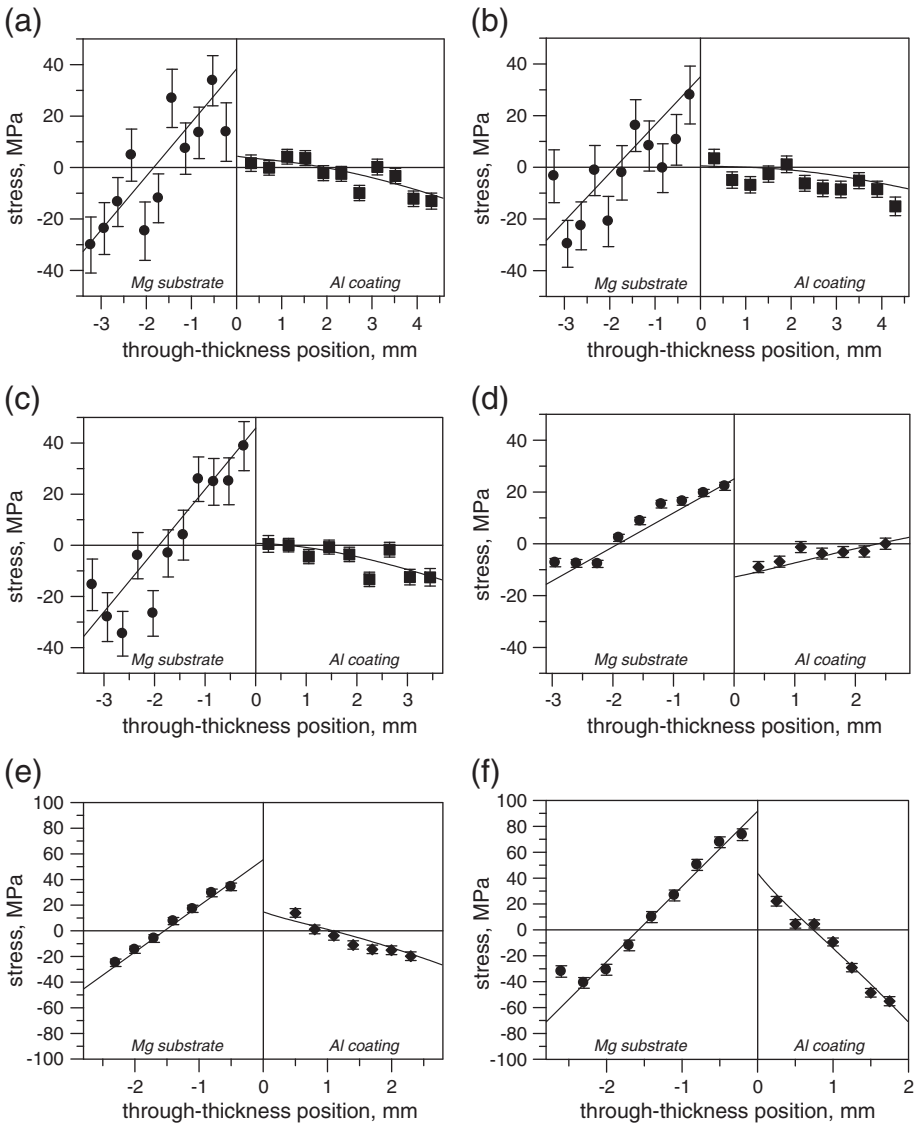

Fig. 3. Stress profiles in Al cold spray coatings. Symbols are the measured values, and solid lines are the progressive deposition model fit [18]. (A) KM Pure Al, He 132°C (B) KM Pure Al, He, 77°C (C) KM Pure Al, N_2 217°C (D) CGT Pure Al (E) CGT 6061Al (F) CGT 7075Al.

on the substrate and coating thickness. However, the value of σ_d represents the amount of residual stress, independent of sample geometry. For this reason, σ_d is used to describe the residual stress behaviour. Considering only the σ_d values as being descriptive of the cold spray process, Table 4 represents the relative amount of peening that has taken place in the formation of the coatings. The three KM coatings all have a similar value, while the two CGT alloy coatings have a higher σ_d value, in particular the 7075 alloy, which has a very large σ_d value.

The residual stress profile in the pure Al CGT coating appears to be an outlier, since it has the lowest σ_d value and the largest $\Delta\varepsilon$ value; however, this is consistent with the higher spray temperature used (see Table 1) and the following considerations. Although the nozzle temperature of 550 °C is an upper bound estimate of the particle temperature upon impact, it is a good indication that the particle temperature is close to that of stress relief or annealing temperatures (~415 °C). Also, the smaller particle size (15 μm vs. 45 μm) results in a higher particle velocity, and will also enable the particle temperature to more closely approach the gas temperature before impact with the substrate (see Table 5). Thus, conditions in this case are such that stress relaxation processes can be dominant during spraying, resulting in very a small residual deposition stress. Here the thermal mismatch is the largest, because the temperature drop after spraying due to the high spray temperature.

Table 4
Fitting parameters of the model [18] and the quality of fit of the experimental data.

	Coating	$\sigma_d \pm$ error, MPa	$\Delta\varepsilon_d \pm$ error, x10^{-6}	$\Delta\varepsilon_{th} \pm$ error, x10^{-6}
1	KM Al (He; 132 °C)	−17 ± 7	−620 ± 120	−340 ± 210
2	KM Al (He; 77 °C)	−20 ± 7	−730 ± 120	−310 ± 200
3	KM Al (N_2; 217 °C)	−21 ± 7	−910 ± 150	−400 ± 240
4	CGT Al	−8 ± 2	−250 ± 30	−450 ± 80
5	CGT 6061Al	−35 ± 6	−1130 ± 100	−330 ± 170
6	CGT 7075Al	−76 ± 7	−2170 ± 100	−220 ± 200

In contrast to the experimental approach of studying residual stress accumulation on a macroscopic level, to describe the cold spray process on the microscopic level a numerical estimate was used. Table 5 gives estimates of the impact parameters for the different materials and process conditions. The impact speed was estimated as described in Section 2.1, and the average impact strain is that already quoted based on metallographic measurements. The calculation of impact duration assumes linear deceleration of the particle on impact [23], as occurs in the Taylor impact test. The strain and

Table 5
Estimated impact parameters based on linear momentum transfer.

	Coating	Calculated Impact Speed [m/s]	Average Impact Strain	Impact Duration [s]	Average Strain Rate [s^{-1}]	Average Impact Pressure [MPa]	Maximum Impact Pressure [MPa]
1	KM Al (He; 132 °C)	585	0.47 ± 0.16	$1.91x10^{-8}$	$2.44x10^{7}$	828	4519
2	KM Al (He; 77 °C)	555	0.43 ± 0.17	$1.88x10^{-8}$	$2.27x10^{7}$	799	4272
3	KM Al (N_2; 217 °C)	352	0.47 ± 0.17	$3.21x10^{-8}$	$1.47x10^{7}$	296	2645
4	CGT Al	805	0.47 ± 0.16	$1.32x10^{-8}$	$3.31x10^{7}$	1650	6400
5	CGT 6061Al	615	0.53 ± 0.23	$4.01x10^{-8}$	$8.80x10^{6}$	828	4784
6	CGT 7075Al	635	0.49 ± 0.22	$3.06x10^{-8}$	$8.94x10^{6}$	971	5153

impact duration give the average strain rate, assuming uniaxial compression of the spherical particle to an oblate spheroid. The average impact pressure is calculated based on linear momentum transfer over the impact time, as done in [24]. This is a useful way of estimating the average pressure seen by the entire particle after its initial impact, followed by subsequent impact by other incoming particles. The maximum impact pressure, on the other hand, neglects the impact time. It is calculated based on momentum transfer from a moving plate of Al, to a fixed, stationary plate of the same material [23].

The maximum impact pressure gives a rough estimate of whether or not deformation propagates through the sample in the form of a plastic shock wave. As the values in Table 5 for maximum impact pressure are well above the Hugoniot elastic limit for Al of ~600 MPa, it is probable that plastic deformation propagated through the particles in the form of a shock wave, at least initially. Since the impacting particles are spherical, attenuation of the shock waves means it is unlikely that the entire particle will deform plastically on impact; rather, the observed deformation is obtained when the particle is subsequently impacted by other particles, to arrive at a final, deformed state. The average impact pressure roughly incorporates these effects.

When looking at different Al coatings, the CGT samples all have a higher impact pressure and impact velocity than the KM samples. This correlates well with the density and Young's modulus data, which are the quantitative measure of compaction. Although the magnitude of the average strain is similar in all cases, it is apparent that the impact pressure is more important for the compaction process, and that is why the density and Young's modulus of the Al sprayed using the CGT system are much closer to their bulk equivalents. The higher values of the Young's modulus for the CGT samples also suggest that the higher impact pressure in the CGT spraying process promotes better bonding, *via* the formation of clean particle interfaces with conformal contact. This is consistent with various numerical simulations which suggest there is a large strain gradient at the particle boundaries, *e.g.*, [25–29]. These simulations also suggest there may be large local temperature gradients.

To make a connection between the macroscopic residual stress profiles and particle deformation on a microscopic scale, we employ an approach used earlier, making an analogy to the shot peening process [5–8]. The main idea is that knowing the average plastic strain of the particles and the elasto-plastic properties of material, the residual stress can be estimated, assuming Hertzian contact, and plastic deformation evolution during both loading and unloading. Another key simplification is that we operate with average, uniform deformation of the material, while in reality a particle experiences several deformation episodes, first when a particle deforms on impact, and then through the impact of successive particles over the course of spraying. Despite this obvious simplification and neglect of parameters such as the variation of temperature in position and time, and the temperature and rate dependence of the yield stress, the model can provide a rough numerical estimate of the residual stress value. This approach assumes that the final amount of plastic deformation is more important than the deformation sequence, and the end result is two key expressions [6]:

$$\sigma_{\max} = -(0.333 + 0.286\alpha\beta)(1-\alpha\beta)[(1-2\alpha\beta)\sigma_s + k\cdot\alpha\beta\cdot p_{\max}] \quad (1)$$

$$p_{\max} = \frac{2}{\pi}\left(\frac{5}{4}\pi E_*^4 \rho V^2\right)^{1/5} \quad (2)$$

Where σ_{max} is the maximum residual stress, p_{max} is the maximum pressure calculated on the assumption of Hertzian contact, σ_s is the yield stress, ρ is the density, V is the impact velocity of the particle, E_* is the equivalent modulus, $E^* = E/2(1-\nu^2)$, and k is a constant close to 1.

Two parameters, α and β, are coupled into a product that describes in simple terms the elasto-plastic state of the deformed material: α is the ratio of the strain hardening rate (tangent modulus) to the Young's modulus, and β is the ratio of the true plastic strain to the true elastic strain.

As can be seen from (1) and (2), the impact stress is the result of several competing factors: spray kinetic conditions (ρV^2), elastic material properties (E, ν), and plastic material properties ($\alpha\beta$ and σ_s). The input parameters in (1) and (2) are readily determined. The average impact pressure from Table 5 is used for p_{max} in (2), in order to roughly account for plastic shock wave attenuation effects.

Here, the most important prediction is a strong dependence of the residual stress on the yield stress, while dependence on other parameters such as $\alpha\beta$ is comparatively weak – especially since the Young's modulus is similar in all cases. Even more precisely, for the conditions of cold spray when $\alpha\beta$ is small, Eq. (1) reduces to $\sigma_{max} \approx 0.333\sigma_s$, *i.e.* the residual stress is approximately 1/3 of the yield stress. As indicated above, the exact value of the yield stress is unknown because of local temperature variations during impact, combined with temperature and rate sensitivity effects. This is expected to result in a non-uniform plastic strain distribution within a deformed particle, and the deformed material cannot be considered to have a single yield stress. However, an effective yield stress can be used to account for non-uniformity effects. Using the model, the effective yield stress can be back-calculated using the measured residual stress in the coating. The result is given in Table 6, and is compared with the yield

Table 6
Estimated surface residual stresses with input parameters.

	Coating	Conditions	Nominal Yield Stress [MPa]	$\alpha\beta$	Measured Residual Stress [MPa]	Effective Yield Stress [MPa]
1	KM Al	(He; 132 °C)	105	0.01	−17 ± 7	50
2	KM Al	(He; 77 °C)	105	0.01	−20 ± 7	50
3	KM Al	(N_2; 217 °C)	105	0.01	−21 ± 7	50
4	CGT Al	(N_2; 550 °C)	105	0.01	−8 ± 2	15
5	CGT 6061Al	(N_2; 400 °C)	260	0.01	−35 ± 6	100
6	CGT 7075Al	(N_2; 400 C)	450	0.01	−76 ± 7	220

stress values of the Al alloys in normal conditions (low-rate deformation at room temperature).

The values in Table 6 show the expected correlation between the nominal yield stress and the effective yield stress, *i.e.* the measured residual stress. As would be expected, the effective yield stress decreases due to the temperature dependence of the yield stress. It reduces by the factor of ~2 for the samples sprayed at lower-temperatures (100 - 400 °C), but it can be as high as ~7 for samples sprayed high-temperature (~550 °C). Based on the experimental results and model considerations, the plastic properties of the coating material are the most significant factor in the accumulation of the compressive peening residual stresses.

5. Conclusions

(1). The density and Young's modulus of the coatings correlate well with the impact pressure and velocity of the samples. In the CGT samples the density and Young's modulus are closer to their bulk equivalents than in the KM samples.

(2). With the exception of the pure Al CGT coating, the residual stress profile is dominated by the peening process. The contribution of thermal mismatch is not significant. The stress profile in the pure Al CGT coating is likely due to the higher spray temperature used, leading to a greater contribution of thermal mismatch to the residual stress profile.

(3). The effective yield stress backed out of the model based on shot peening scales with the process temperature in the case of the pure Al samples, and with the plastic properties of the material, when comparing the alloys.

Acknowledgements

Funding for this project through the Australian Research Council Centre of Excellence for Design in Light Metals is gratefully acknowledged. Travel and accommodation support for the neutron diffraction stress measurements was generously provided by The Australian Institute of Nuclear Science and Engineering (AINSE).

References

[1] D.J. Greving, J.R. Shadley, E.F. Rybicki, J. Therm. Spray Technol. 3 (1994) 371.
[2] R. McGrann, D. Greving, J. Shadley, E. Rybicki, B. Bodger, D. Somerville, J. Therm. Spray Technol. 7 (1998) 546.
[3] S.J. Howard, Y.C. Tsui, T.W. Clyne, in: C.C. Berndt, S. Sampath (Eds.), 1994 Thermal Spray Industrial Applications, Proceedings of the 7th National Thermal Spray Conference, 20–24 June 1994, ASM International, Materials Park, Ohio, Boston, Massachusetts, 1994, p. 703.
[4] S. Sampath, X.Y. Jiang, J. Matejicek, L. Prchlik, A. Kulkarni, A. Vaidya, Mater. Sci. Eng. A 364 (2004) 216.
[5] V. Luzin, K. Spencer, M.X. Zhang, Acta Mater. 59 (2011) 1259.
[6] K. Ogawa, T. Asano, Mater. Sci. Res. Int. 6 (2000) 55.
[7] J.K. Li, M. Yao, D. Wang, R. Wang, Mater. Sci. Eng. A A147 (1991) 167.
[8] A.S. Franchim, V.S.D. Campos, D.N. Travessa, C.D.M. Neto, Mater. Des. 30 (2009) 1556.
[9] V. Champagne, J. Fail. Anal. Prev. 8 (2008) 164.
[10] M. Campo, M. Carboneras, M.D. López, B. Torres, P. Rodrigo, E. Otero, J. Rams, Surf. Coat. Technol. 203 (2009) 3224.
[11] R. Dykhuizen, M. Smith, J. Therm. Spray Technol. 7 (1998) 205.
[12] C.B. Henderson, AIAA J. 14 (1976) 707.
[13] ASTM Standard E1876-09, Standard Test Method for Dynamic Young's Modulus, Shear Modulus, and Poisson's Ratio by Impulse Excitation of Vibration, ASTM International, West Conshohocken, PA, 2009.
[14] ASTM Standard D6272-10, Standard Test Method for Flexural Properties of Unreinforced and Reinforced Plastics and Electrical Insulating Materials by Four-Point Bending, ASTM International, West Conshohocken, PA, 2010.
[15] J.C. Russ, R.T. Dehoff, Practical Stereology, Second edition Kluwer Academic/Plenum, New York, 2000.
[16] W.B. Choi, L. Li, V. Luzin, R. Neiser, T. Gnaupel-Herold, H.J. Prask, S. Sampath, A. Gouldstone, Acta Mater. 55 (2007) 857.
[17] E. Kröner, Z. Phys. 151 (1958) 504.
[18] Y.C. Tsui, T.W. Clyne, Thin Solid Films 306 (1997) 23.
[19] S.J. Howard, Y.C. Tsui, T.W. Clyne, Acta Metall. Mater. 42 (1994) 2823.
[20] K. Spencer, D.M. Fabijanic, M.X. Zhang, Surf. Coat. Technol. 204 (2009) 336.
[21] Y. Tao, T. Xiong, C. Sun, H. Jin, H. Du, T. Li, Appl. Surf. Sci. 256 (2009) 261.
[22] E. Irissou, J.-G. Legoux, B. Arsenault, C. Moreau, J. Therm. Spray Technol. 16 (2007) 661.
[23] M.A. Meyers, Dynamic Behavior of Materials, John Wiley & Sons, Inc., New York, 1994, p. 669.
[24] T.H. Van Steenkiste, J.R. Smith, R.E. Teets, Surf. Coat. Technol. 154 (2002) 237.
[25] S. Yin, X.-F. Wang, W.-Y. Li, B.-P. Xu, J. Therm. Spray Technol. 18 (2009) 686.
[26] T. Schmidt, H. Assadi, F. Gärtner, H. Richter, T. Stoltenhoff, H. Kreye, T. Klassen, J. Therm. Spray Technol. 18 (2009) 794.
[27] W.-Y. Li, H. Liao, C.-J. Li, H.-S. Bang, C. Coddet, Appl. Surf. Sci. 253 (2007) 5084.
[28] T. Schmidt, F. Gartner, H. Assadi, H. Kreye, Acta Mater. 54 (2006) 729.
[29] H. Assadi, F. Gartner, T. Stoltenhoff, H. Kreye, Acta Mater. 51 (2003) 4379.